Hatala, KG, Gatesy, SM and Falkingham, PL

Integration of biplanar X-ray, three-dimensional animation and particle simulation reveals details of human 'track ontogeny'

Integration of biplanar X-ray, 3-D animation, and particle simulation reveals details of human 'track ontogeny'

Kevin G. Hatala[1]*, Stephen M. Gatesy[2], Peter L. Falkingham [3]

[1]Department of Biology, Chatham University

[2]Department of Ecology and Evolutionary Biology, Brown University

[3]School of Biological and Environmental Sciences, Liverpool John Moores University

*Corresponding author (E-mail: kevin.g.hatala@gmail.com)

Abstract

The emergence of bipedalism had profound effects on human evolutionary history but the evolution of locomotor patterns within the hominin clade remains poorly understood. Fossil tracks record the anatomy and kinematics of extinct hominins, and they offer great potential to reveal locomotor patterns at various times and places across the human fossil record. However, there is no consensus on how to interpret anatomical or biomechanical patterns from tracks due to limited knowledge of the complex foot-substrate interactions through which they are produced. Here we implement engineering-based methods to understand human track formation and potentially unlock invaluable information on hominin locomotion from fossil tracks. We first developed biplanar X-ray and 3-D animation techniques that permit visualisation of subsurface foot motion as tracks are produced, and that allow for direct comparisons of foot kinematics to final track morphology. We then applied the discrete element method to accurately simulate the process of human track formation, allowing for direct study of human track ontogeny. This window lets us observe how specific anatomical and/or kinematic variables shape human track morphology, and it offers a new avenue for robust hypothesis testing in order to infer patterns of foot anatomy and motion from fossil hominin tracks.

Keywords: hominin footprints, trace fossils, locomotion, discrete element method

Introduction

Central to the study of human evolution are questions concerning the evolution of our unique form of bipedal locomotion. While bipedalism has long been considered a defining trait of the hominin clade (1), discoveries within the past half-century have made it apparent that

multiple forms of bipedalism likely existed among fossil hominins. Some of these forms were probably quite similar to our own bipedal locomotion but others were almost certainly quite different (2). To date, most evidence for the inferred locomotor patterns of fossil hominins has come from comparative morphological studies of postcranial skeletal fossils. However, fossil hominin tracks (i.e., footprints) have augmented, and have the potential to further augment, these comparative osteological studies in important ways.

Tracks offer the only data on whole-foot anatomy, foot posture, and foot kinematics in fossil hominins. Fossil hominin foot bones are most often found in isolation and even the most exceptional, "nearly complete" hominin foot skeletons are missing important elements (e.g., OH 8 [*Homo habilis* (3)]; LB1 [*Homo floresiensis* (4)]; Foot 1 [*Homo naledi* (5)]; DIK-1-1f [*Australopithecus afarensis* (6)]). Tracks are morphological features that result from the dynamic interaction between the composite foot morphology (articulated foot skeleton and its soft tissues) and a deformable substrate. Understanding, or reverse-engineering this interaction means tracks can offer a picture of extinct hominin foot morphology complimentary to that offered by the bones alone. At the same time, tracks record the three-dimensional kinematics of feet as they navigated deformable substrates (7), allowing one to observe foot postures and motion patterns that were actually used during bouts of terrestrial bipedalism. While the articular surfaces of skeletal fossils might provide rough estimates of maximal joint mobility (but see (8)), tracks result from specific poses and motion sequences that can help one to understand how hominin feet were actually used to accomplish particular forms of bipedal locomotion.

In addition to tracks being able to augment analyses of skeletal fossils in critical ways, fossil hominin track sites have been discovered at a high rate in recent years. The known record of hominin track sites that predate modern humans has experienced notable growth (9–15). In

some cases, the known sample sizes of hominin tracks now exceed by more than an order of magnitude the sample of hominin foot skeletal fossils from the same time periods (12). New technologies are also being applied to digitally record hominin tracks in 3-D, thereby opening doors for digital preservation, data sharing, and computational analyses (16,17).

Yet despite the great potential of these data and numerous recent advances in hominin ichnology, there still exist major obstacles that limit access to the invaluable information preserved by fossil hominin tracks. Perhaps the most important obstacle is our currently limited understanding of the complex interactions between foot anatomy, kinematics, and substrate through which a track is formed (18–20). Morse et al. (21) demonstrated, through a case study of Holocene human tracks from Namibia, that track morphology can vary substantially as the same individual walks through substrates of different consistencies. Yet the underlying reasons for that variation remain unknown. Deciphering the mechanical nature of foot-substrate interactions is essential for linking aspects of track morphology to anatomical or kinematic patterns (19) and thereby for leveraging hominin tracks to better understand the evolution of human foot anatomy and locomotion.

Falkingham and Gatesy (22) coined the term “track ontogeny” to describe the mechanical process through which tracks are formed. This term emphasizes the fact that track morphology develops through a dynamic sequence of continuous interactions between foot and substrate. This developmental sequence is inherently difficult to study because track creation is usually hidden from view – both human feet and natural substrates are opaque and so their interactions cannot be observed directly. Building upon earlier biomechanical and robotic studies that used X-rays to visualize subsurface motion (e.g., 23), Ellis and Gatesy (24) and Falkingham and Gatesy (22) introduced biplanar X-ray approaches for studying 3-D foot-substrate interactions

that result in track formation. Those studies focused on track formation in guineafowl, but their biplanar X-ray approach was more recently adapted and applied to study track formation in humans (25).

Falkingham and Gatesy (22) were also the first to use particle simulation to understand track ontogeny, by using the Discrete Element Method (DEM) to examine the mechanistic origins of track morphology. The DEM simulates individual sediment particles as they interact with each other and external geometry. These particle interactions are governed by physical parameters including elasticity, compressibility, cohesion, and mass (26,27). By iteratively simulating track formation processes, with consistent validation using experimental data, Falkingham and Gatesy (22) and Falkingham et al. (28) were able to leverage their ontogenetic perspective to develop robust inferences of trackmaker foot anatomy and foot kinematics from fossil dinosaur tracks.

Here, we present the development and first application of similar methods that employ biplanar X-ray, 3-D animation, and particle simulation to study track ontogeny in humans walking through deformable muds. We build on existing methods in important ways, most notably by animating and simulating high-resolution deformable 3-D models of human feet as they interact with deformable substrates. We present a case study in which we demonstrate the application of new methods, and potential directions for future research. These methods allow us to open the black box of the foot-substrate interactions through which tracks are formed, and they provide an avenue for robust inferences of foot anatomy and kinematic patterns to be derived from fossil hominin tracks.

Methods

Biplanar X-ray experiments

Subjects

The methods presented here were developed and applied through experiments with four healthy adult volunteer subjects, though as a proof of concept we present focused analyses from only one individual. Subjects were recruited and provided informed consent to participate through protocols approved by the Institutional Review Boards of Chatham University and Brown University.

Biplanar X-ray setup and technique

The biplanar X-ray equipment, and its configuration within the W.M. Keck Foundation XROMM Facility at Brown University closely followed that used by Hatala et al. (25). Details on this configuration and recording settings are provided in Supplementary Text S1.

Trackway and substrates

A roughly 6-meter long (~60 cm wide, ~50 cm tall) elevated trackway was assembled, following a setup that we have used previously to study human track formation via biplanar X-ray (25). The biplanar X-ray apparatus was configured at roughly the center of this trackway, with the two X-ray beams at an angle of approximately 90 degrees to each other. To improve visibility of markers on the sole of the foot, the X-ray beams were pitched upwards 10 degrees relative to the ground plane. X-ray emitters and image intensifiers were placed with a source-to-image distance of 134 cm. X-ray videos captured anteromedial and anterolateral projections of subjects feet.

The trackway was configured such that different substrates of interest could be placed within the area of biplanar X-ray overlap. A modified stone slab table formed a rigid and stable base within this central portion of the trackway. Three rigid, closed-cell foam panels (two 2-inches thick, one 1-inch thick) were placed on top of the stone slab, and a diamond-shaped recess was cut in the center of them, providing a space in which an interchangeable substrate container could be securely placed (Fig. 1).

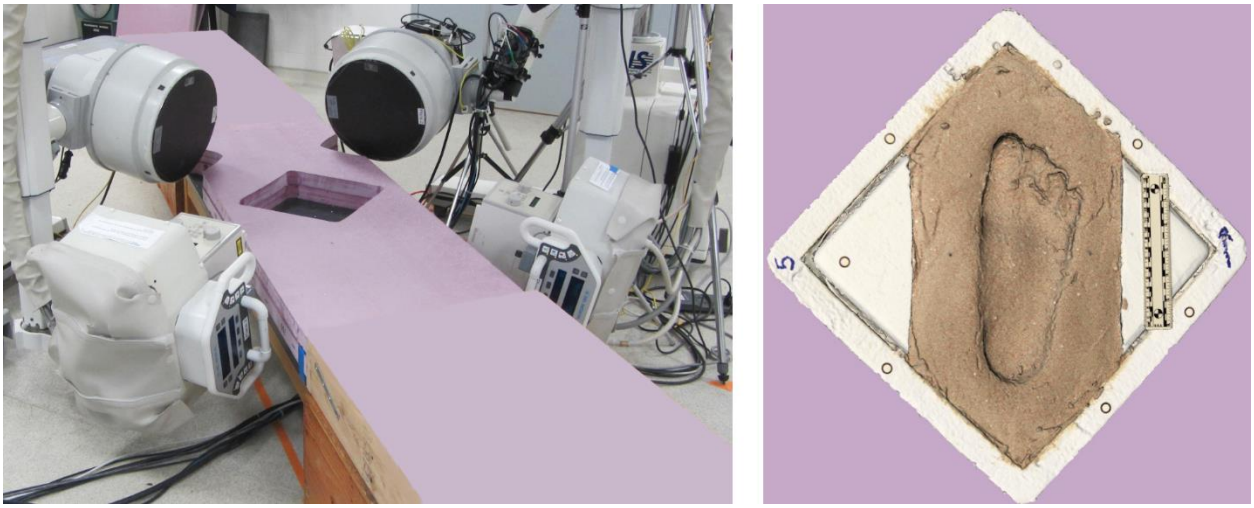

Figure 1. Edited photo showing trackway and biplanar X-ray configuration used in track formation experiments. Portions of the trackway preceding and following the central, substrate-bearing section were covered with various foams to make the entire trackway level and equally deformable under each substrate condition. The central section includes a diamond-shaped recess into which substrate containers were placed. The panel on the right shows an overhead view of a 3-D scan of the substrate container, with a track produced within it (in “hydrated 5” mud).

This configuration allowed for the study of foot motion on four substrates. In one setup, a rigid foam core carbon fiber panel (79 x 30.5 x 2.7 cm) was placed over top of the recess, and 1-

inch closed-cell foam panels were placed along the remaining length of the trackway in order to make it level. In the remaining three setups, a square foam container (30 cm by 30 cm opening, 14.5 cm deep, with 3 cm walls) was placed within the recess. Foam wedges were placed in the medial and lateral corners of the substrate container, in order to reduce the volume of "unnecessary" mud that X-rays would have to traverse but that would not interact with the foot (thereby improving clarity of the X-ray videos). This left an area 22 cm wide, which held one of three varieties of mud into which the foot would impress (Fig. 2). In these configurations, the remainder of the trackway was topped with panels of rigid, closed-cell foam (for "firm" mud, described below) or soft, deformable upholstery foams (approximately 2.5 cm thick for "hydrated 2.5" mud, 5 cm thick for "hydrated 5" mud, described below) to mimic the deformative natures of the substrates of interest and provide a level surface along the entire trackway length.

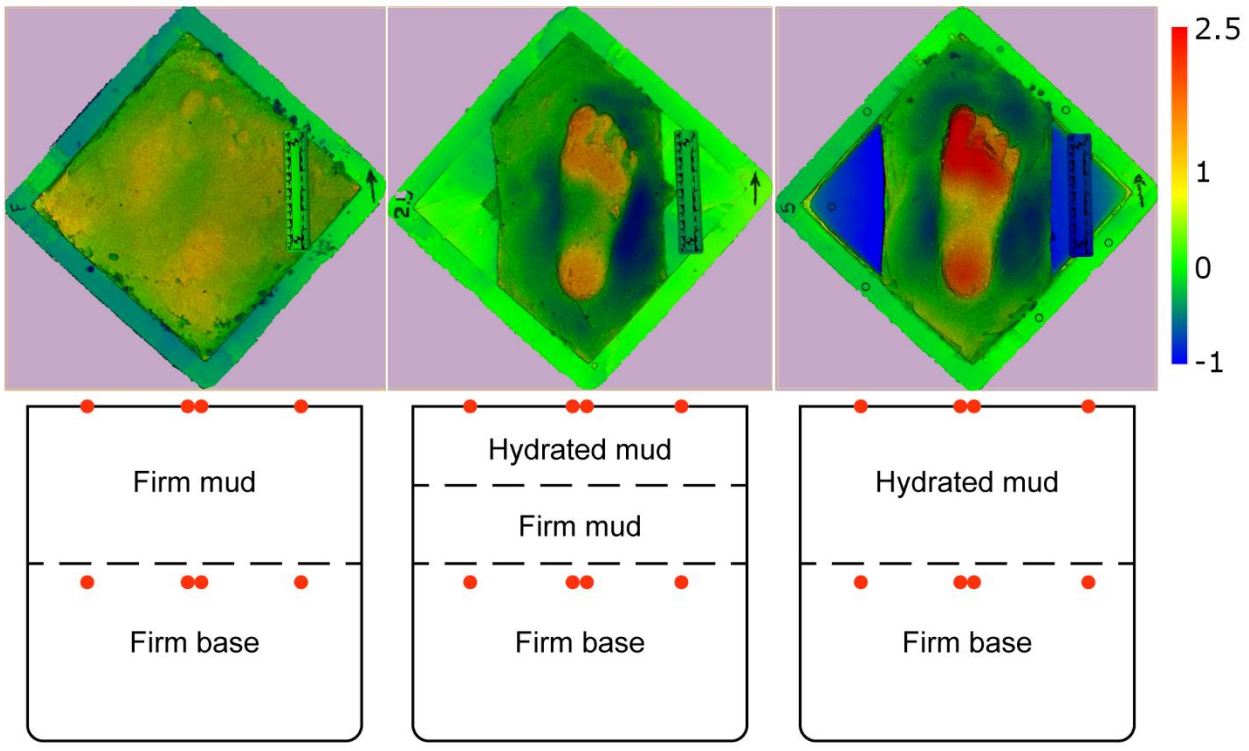

Figure 2. Side-by-side comparisons of 3-D track models from the same subject in the three varieties of mud (top row), alongside schematics showing the contents of substrate containers (bottom row). Substrates included "firm" mud (left), "hydrated 2.5" mud (center), and "hydrated 5" mud (right). Track depth is reflected by color gradients according to scale at far right, which is displayed in centimeters. Each substrate container included 6.5 cm of "firm base", and an overlying 5 cm that was filled according to the substrate conditions of that particular trial. At the locations of orange dots, radiopaque marker beads were placed within and upon each substrate in diamond-shaped patterns, to align the final track model within the same calibrated space as the foot during 3-D animation.

Building upon previous biplanar X-ray studies of track formation (22,25,29), we developed a new range of radiolucent, deformable, and cohesive muds that mimic the mechanical behaviors and particle dimensions of naturally-occurring muds. These muds consisted of 60 micron glass bubbles (Type K15, 3M Co., St. Paul. MN, USA), modeling clay, water, and acrylic blast media (Type V, 0.42-0.56 mm diameter; Kramer Industries, Inc., Piscataway, NJ, USA). The first three ingredients were mixed in a 24:5:9 volumetric ratio (following (29)) and this combination was then mixed with the acrylic blast media in roughly equal volumetric proportions. In filling the substrate containers with mud, a substantial base portion of substrate would not interact directly with subjects' feet. In the bottom-most 6.5 cm of substrate, we integrated EPS foam pellets (2-4 mm diameter; LACrafts) with the above ingredients, to further enhance radiolucency while still maintaining relatively consistent material properties throughout the substrate volume. Slightly beneath the surface of this firm base we placed four radiopaque markers 3 mm in diameter, such that we could track those points and

identify and account for any potential disturbance to the entire substrate volume. The remaining 5 cm were then filled with one of three mud variants. In the "firm" mud condition, the substrate container was filled to the rim with acrylic mud and tightly packed by tamping with a rubber mallet. In the "hydrated 2.5" condition, 2.5 cm of "firm" mud was added atop the firm base. Water was added to acrylic mud to make it more fluid and deformable and this filled the most superficial 2.5 cm of the substrate container.. In the "hydrated 5" condition, the entire most superficial 5 cm of the substrate container was filled with the hydrated acrylic mud. On the surface of each of these substrates, we again placed four radiopaque beads 3 mm in diameter, such that we could use those points to register the position of the final track during 3-D animation (Fig. 2).

Experimental protocol

Subjects had an array of 85 radiopaque beads placed on the external surface of their right foot, the motions of which could be tracked via biplanar X-ray. Some of these markers were placed at anatomical locations of interest, but others filled in gaps to provide a roughly uniform mesh of markers across the entire plantar surface of the foot. This array of bead markers expands upon a 70 marker array used in earlier experiments (25) to achieve even more complete surface coverage. Before marker beads were placed, a template was drawn on each subject's foot using semi-permanent marker. The foot was then 3-D scanned at 1.0 mm resolution using a handheld structured light scanner (Creaform Go!SCAN 50, Creaform, Lévis, Québec, Canada; Fig. 3). Following scanning of the foot with its marker template, 1.5-mm diameter radiopaque markers (SureMark, Simi Valley, CA, USA) were placed and secured using medical adhesive (SkinTac^{TM}, Torbot, Cranston, RI, USA). After markers were placed, subjects moved to the

experimental trackway and walked across it several times until they were fully comfortable moving within that environment.

Figure 3. High-resolution 3-D scan of a subject's foot with template for marker placements drawn in semi-permanent marker. Views are plantar (center), lateral (left), medial (right), dorsal (top). No markers were placed on the dorsum of the foot aside from those on the dorsal sides of the toes.

Subjects traversed the experimental trackway for at least 13 trials each. In one trial, the subjects simply stood with their right foot on the carbon fiber plate (with their left foot immediately behind for support) while a single pair of X-ray images were taken of their "statically loaded" marked foot. Each subject then walked across each of the four substrates (carbon fiber and the three mud variants) for at least three trials at their self-selected comfortable walking speed. If their foot strayed outside of the biplanar X-ray view, they were asked to repeat that trial. For trials in which subjects walked through mud, the track they created was 3-D scanned. For most trials the structured light scanner was used to scan the track at 1.0 mm resolution. However, there were nine trials in which the scanning software was still processing the model from the previous trial, and therefore we scanned tracks using photogrammetry (Canon 5D Mark III camera, Canon, Melville, NY, USA; Agisoft Metashape Professional v.1.6.4, Agisoft LLC, St. Petersburg, Russia). After track scanning, the substrate was reconfigured to its initial state using a trowel, or swapped for a different substrate before the next trial.

Motion tracking and 3-D animations

XMALab software (v.1.5.5) was used to compute the 3-D trajectories of radiopaque marker beads that were placed on the foot, as it moved on and within the substrates of interest. Following protocols that were established for X-Ray Reconstruction of Moving Morphology (30,31), XMALab was used to remove distortion from video recordings, calibrate the 3-D volume in which biplanar X-rays overlapped, and then track marker trajectories in 3-D. Since our markers were placed on non-rigid human feet, and we sought to track soft tissue deformations and motions, there was no informed basis for applying a filter to these data. Further, we used

XMALab's polynomial fitting procedure to improve sub-pixel accuracy (a procedure that has been shown to reduce standard deviations of inter-marker distances on rigid bodies (31)), and recorded at speeds of only 50 Hz, which should have the effect of minimizing potential "noise" in 3-D marker trajectories. Additional details regarding marker tracking are provided in Supplementary Text S2.

High-resolution scans of subjects' feet were processed and cleaned using Creaform VXElements software (v. 7.0.1). Built-in mesh editing features were used to remove noisy polygons (i.e., those discontinuous with the foot model) and to trim the foot model such that it included, in general, only the area distal to the medial and lateral malleoli. These 3-D models were exported in .obj format and then imported in Autodesk Maya 2020 for animation.

In the animation protocol, the high-resolution foot mesh was first imported to Autodesk Maya 2020. For each individual trial, the 3-D coordinates of foot markers were imported into Maya and animated as a collection of spheres each 1.5 mm in diameter using the "imp" function of XROMM MayaTools (v. 2.2.3) (32). The positions of these spheres were linked to the positions of the bead markers on the surface of the high-resolution foot model (Fig. 3; Supplementary Text S3). The spheres were inter-connected such that their motions moved the vertices of a low-resolution mesh, which in turn drove motions of the high-resolution mesh using Maya's wrap deformer function (Supplementary Text S3, Supplementary Figure S1). Through this series of connections and deformations, biplanar X-ray data were used to create trial- and subject-specific animations of both aerial and sub-surface skin movements during track formation (Fig. 4).

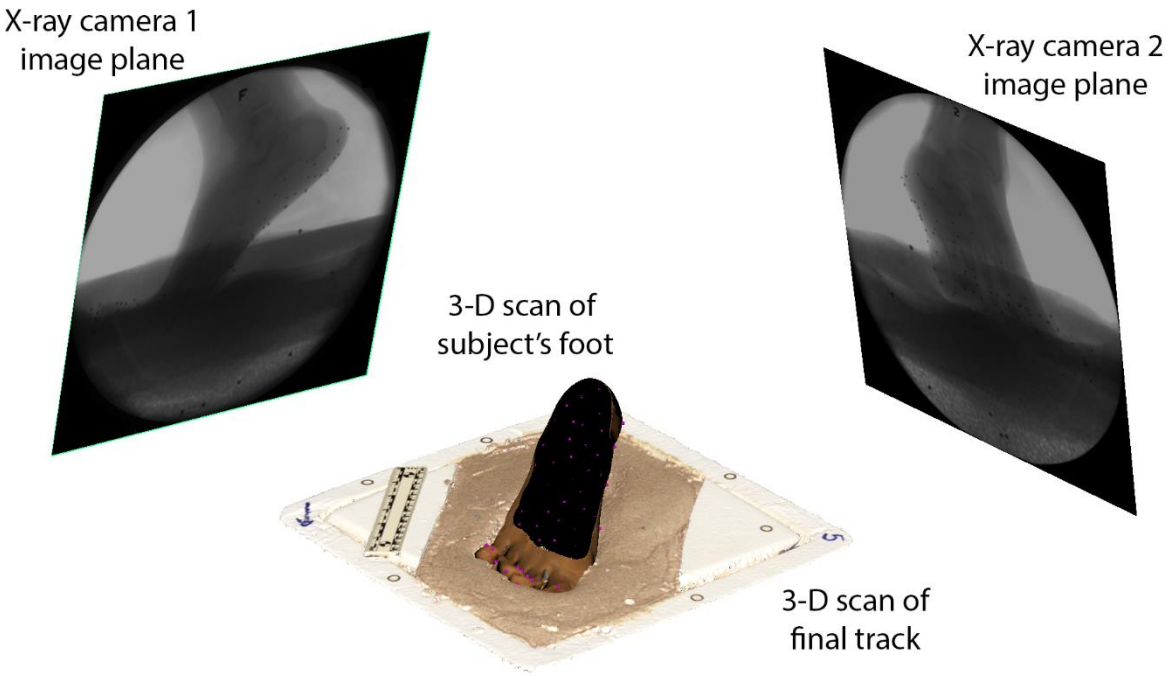

Figure 4. Snapshot of an animation of a single trial from biplanar X-ray experiments. The position of the mobile and deformable high-resolution 3-D foot scan is continuously guided by the tracked 3-D positions of external foot markers. Markers on the external surface of the foot appear as black dots in X-ray camera views, and are highlighted in purple for the sake of visibility on the animated foot model.The foot animation is integrated with a 3-D model of the final track that was produced in this trial, registered within the same calibrated 3-D space. Integration of feet and tracks within the same animation scene allows for direct visualization of the correspondence between track morphology and pedal kinematics.

Spheres (3.0 mm in diameter) were also animated to represent markers placed within and upon the substrate (Fig. 2). The final configuration of the four markers visible on the tracked surface were used to translate and rotate the scan- or photogrammetry-derived 3-D track model into registration. Such registration is critical for assessing the correspondence (or lack of correspondence) between pedal kinematics and track morphology. However, because only the

final track was captured, the integration of a dynamic foot with a static footprint (Fig. 4) is insufficient to fully explain the origin and modification of specific features during a step. For insights into the interplay between foot shape, foot motion, and substrate displacement, we turned to simulation.

Simulating track formation

We used LIGGGHTS (www.cfdem.com; 27) to carry out discrete element simulations of foot-substrate interactions. Our simulation process began with relatively simple foot motions and iteratively increased motion complexity, in line with the animation process outlined above. All simulations used the same initial particle set-up and parameters. A virtual tray 21 cm x 35 cm and 8 cm deep was created in Autodesk Maya in the same world-space position as the original substrate container. This completely encompassed the track-forming volume, though the virtual tray lacked the diamond-shaped ends of the real substrate container for computational simplicity. The virtual tray was filled with ~800,000 particles of 1 mm radius. While this particle size is homogeneous and significantly larger than the experimental substrate, particle properties (Young's modulus, Poisson ratio, cohesion, and friction) were adjusted such that the macroscopic bulk behaviour was similar to our substrate.

The simplest simulation involved a vertical stamping of a rigid foot model (the scan of the subject's foot in resting pose). Sinking depth of the rigid foot was equal to the deepest part of the real moving foot at mid-stance. Timing was such that the indentation and removal of the rigid foot took the same number of frames as the experimental trial being simulated, i.e. the simulated time taken to 'stamp' the rigid foot was equal to the real timing of the original footstep. This most simplistic scenario was followed first by a single rigid foot rotating to approximate a heel-

toe cycle, and then by a two-part foot in which the toes were able to rotate as an object independently of the foot (i.e., with a simple hinge at the approximate positions of the metatarsophalangeal joints). The single rotating foot object was animated to sink in the substrate such that the maximum depth of the metatarsal heads matched the depth of the metatarsal heads in the biplanar X-ray data. While this meant the majority of the foot approximated the motion of the bi-planar X-ray data, the toes necessarily sank much farther due to significant rotation. The two-part model alleviated this by allowing the toes to remain more horizontal as the heel lifted off the substrate. This two-part rigid body simulation is analogous to previous footprint simulation work (22,28) in which individual toe segments were treated as separate translating and rotating rigid bodies.

However, these rigid-body models failed to capture subtle deformations of the human foot, particularly involving flexibility of the arches. Our final simulation used the animated high-resolution foot mesh directly, capturing as much of the reconstructed motion as possible. To do this, mesh face and vertex positions were output at a far greater temporal-resolution; 1000 frames per second. LIGGGHTs input files ran 1000 timesteps (each of 0.000001 seconds real time) between each frame to translate the mesh from one position to the next. This produced the most 'realistic' simulations, incorporating all motion of the deforming foot as derived from the skin markers placed on the subject. Simulations were visualized using OVITO (v. 3.0.0) (33).

Results and Discussion

Using the methods described above, we successfully built data-driven 3-D animations of deformable feet navigating deformable substrates to produce tracks (Supplementary Video S1). Since the methodological developments are the focus of this paper, we present data from a single

subject as a case study to demonstrate the variety of analyses that are permitted through the application of these novel methods.

The first area in which we can apply these techniques is to study 3-D kinematics of the foot at the substrate interface. The biplanar X-ray technique presented here provides a window for direct visualization of the foot-substrate interface while a human foot travels into, and interacts with, both rigid and deformable substrates. As in previous studies (25), the 3-D positions of external foot markers, visualized through biplanar X-ray, can be used to quantify 3-D deformations of the plantar surface of the foot during its interactions with these various substrates. For example, continuous measurements of heel compression, heel expansion, and longitudinal arch deformation can be collected throughout the duration of stance phase to understand soft tissue behavior in these regions of the foot (Fig. 5).

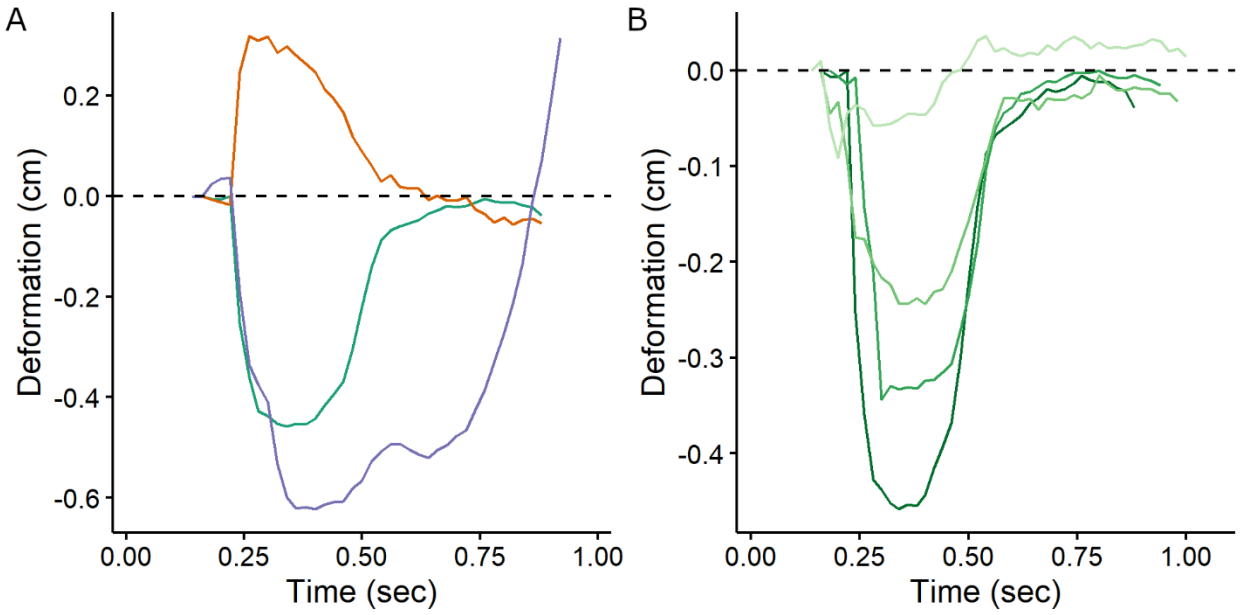

Figure 5. 3-D deformation of the foot of one individual walking across multiple substrates. A) Continuous measurements of heel height (green), heel width (orange), and medial longitudinal arch height (purple) during one trial on carbon fiber. Each measurement is zeroed based on its

first possible measurement (prior to initial contact, when the foot first entered both biplanar X-ray video frames). B) Sample plots showing deformation of the heel (change in vertical height) in one subject walking across four different substrates. Substrates become more deformable as they transition from darker to lighter shades of green (carbon fiber is the darkest green, “firm” mud is the second darkest, “hydrated 2.5” mud is the second lightest, and “hydrated 5” mud is the lightest).

Figure 5 portrays temporal and substrate-driven patterns of foot deformation consistent with those previously observed by Hatala et al. (25). The external surface of the heel simultaneously compressed vertically and expanded horizontally as the calcaneal fat pad dissipated impact forces (Fig. 5A), a pattern which has been well-studied experimentally (34–36). The medial longitudinal arch initially flattened as the foot was loaded, but at terminal stance phase it eventually reached a height that exceeded its initial, unloaded, state (Fig. 5A), consistent with results from other experimental studies of longitudinal arch function (37). Comparisons across substrates likewise followed patterns observed previously by Hatala et al. (25). For example, the heel compressed to greater degrees as subjects walked over more rigid substrates (Fig. 5B). Clearly these are not the only types of dynamic measurements that can be acquired, and a variety of 3-D kinematic studies would be possible through this approach. We simply emphasize here that our experimental protocol offers several directions to study foot-substrate interactions across rigid and deformable substrates using external marker-based kinematics.

Building upon studies of pure foot deformation and motion, the integration of high-resolution 3-D models of both feet and tracks within the same animation scene provides opportunities to observe directly the extent and nature of correspondence between external foot

motions and the morphology of the final track that was produced. Previous studies have highlighted the lack of direct correspondence between foot motion and track morphology (25) and similar patterns were observed here. It is evident that final track morphology is not simply a Boolean-type subtraction of the foot's trajectory through the substrate. While the lack of correspondence between foot trajectories and final track morphology can be observed from the results of 3-D animations of experimental trials, a true understanding of these differences requires knowledge of human track ontogeny. Such knowledge can be gained through track simulations, which allow one to visualize and understand the patterns of substrate flow that generate specific aspects of track morphology. Here we explored as a case study a single trial from our biplanar X-ray experiments, in which a subject walked across "hydrated 5" mud to produce a track. The 3-D scan of that track was directly compared with simulated tracks that were produced following the track simulation protocols described above.

By iteratively increasing the complexity of the deformation and motion of the animated foot, we achieved simulations that eventually produced track morphologies that closely matched those produced in biplanar X-ray experiments (Fig. 6, Table 1). The simplest simulation, in which a rigid foot model vertically stamped a substrate, actually generated a track morphology with the smallest average pairwise distance from the 3-D scanned track (Table 1) and that looked qualitatively realistic. However, the similarities between the simulated and scanned tracks were largely confined to the region of the forefoot (Fig. 6). This was unsurprising, since the simulated foot trajectories were configured such that maximum depth beneath the metatarsal heads matched the depths to which the metatarsal heads were observed to travel in biplanar X-ray experiments (i.e., all simulations are most likely to match the 3-D scanned track in the region of the forefoot). The "vertical stamp" produced a track that was noticeably shallower and narrower

than the scanned track in the region of the heel, and that had an overall less longitudinally arched shape. This track also lacked the displacement rims that surrounded the perimeter of the scanned track.

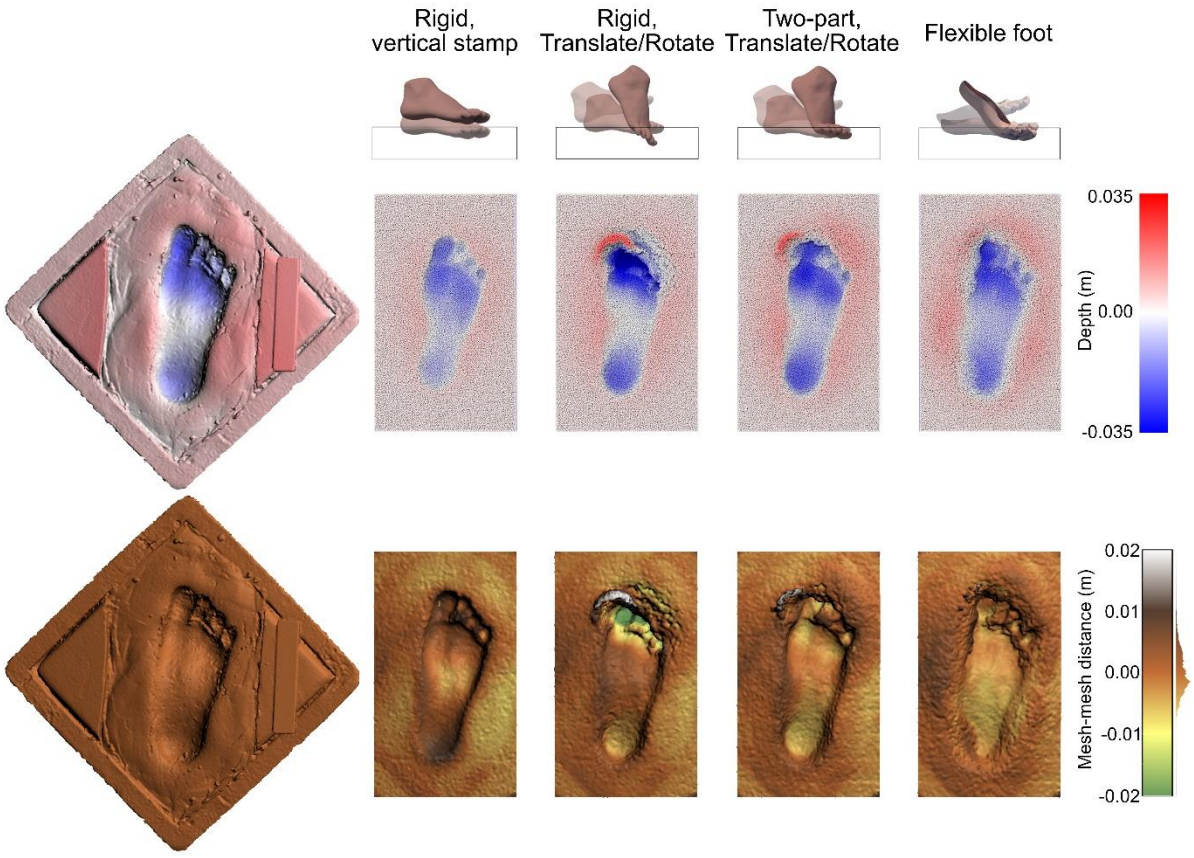

Figure 6. Direct comparisons between 3-D scan of track from biplanar X-ray experiments (left) and 3-D meshes of tracks produced in various particle simulations (right). Simulations increase in complexity from left to right, from a vertical stamp of a rigid foot to a step taken by a fully flexible foot, whose motions and deformations were driven by real data from biplanar X-ray experiments. Top row shows track depths (in meters) as measured from the ground plane. Bottom row shows pairwise distances between each simulated track and the actual 3-D scanned track. Differences between simulation conditions are subtle, but overall the most complicated

422 animation/simulation converges on a track morphology that is most similar to the one actually
423 produced in biplanar X-ray experiments.
424
425 **Table 1**. Summary statistics for pairwise distance comparisons between simulated tracks and 3-
426 D scanned track from biplanar X-ray experiments.

Simulation type	Mean distance (cm)	Standard deviation (cm)
Rigid foot, vertical stamp	0.0062	0.3446
Rigid foot, translate/rotate	-0.0286	0.5980
Two-part foot, translate/rotate	0.0556	0.3511
Fully flexible animated foot	0.0176	0.2885

427
428 By adding motion to the rigid foot model (translating and rotating a rigid foot), we
429 produced simulated tracks that had greater relative elevation beneath the longitudinal arch but
430 that were otherwise quite different from the 3-D scanned track. Toe impressions were extremely
431 deep, the heel impression was deeper than observed in the scanned track, and a very noticeable
432 extrusion feature was generated at the tip of the hallux (Fig. 6). Displacement rims were still not
433 as prominent as they were in the 3-D scanned experimental track. Adding a simple hinge to
434 convert the rigid foot into a two-part model (allowing the foot to deform at the approximate
435 positions of the metatarsophalangeal joints) remedied some but not all of these inaccuracies.
436 Forefoot (including toe) impressions were overall more similar to those of the 3-D scanned track,

but the heel impression was still deeper and the extrusion feature at the tip of the hallux was still generated (Fig. 6).

Implementing a fully mobile and deformable foot animation led to simulated tracks that most closely matched those observed in biplanar X-ray experiments. The mean distance between the simulated and 3-D scanned tracks was only second lowest but the standard deviation was the smallest, indicating that this simulation varied the least of the four scenarios from the original scanned surface (Table 1). The simulated track was similar in relative depths across the forefoot (including toe) impressions, relative depths in the region of the heel, and in the pattern of the displacement rim surrounding the perimeter of the track (Fig. 6). It was also the widest track in the mid-foot, which matched most closely with the real track. The simulated track had a slightly deeper impression beneath the longitudinal arch than did the 3-D scanned track, but this difference was relatively subtle.

It is clear from our simulated tracks that, as might be expected, incorporation of more complex motions and soft-tissue deformations results in a more true-to-life final track morphology. That the real track differed substantially from the 'stamp' simulation demonstrates once again that "footprints are not feet" and should not be interpreted as direct reflections of plantar foot anatomy (29). Our simulated tracks also highlight caution in using simple metrics such as mean mesh-mesh distances to compare tracks; the complex 3D topography means that mean distances can be low, even when tracks are clearly qualitatively different.

Focusing on our most complex simulation (deformable foot), the qualitative and quantitative similarity between simulated track and real scanned track is gratifying, and indicates that the real motions of the foot and substrate are captured by our workflow. Minor differences between the final simulated track and the 3D-scan of the real impression can be attributed to

simulation parameters, particularly particle size and cohesion, though refining these parameters further would require substantial iterative simulations, which for the purposes of this study were deemed unnecessary. The nature of how the sediments are mixed and set-up during the experimental protocol means that the bulk properties of the experimental substrate (particularly as it overlies elastically-behaving foam) would be difficult to ascertain from a smaller, and thus easier to simulate, sample. As such, we base our input parameters on what makes the output most like the scanned track, but as elaborated on previously (28) significant deviations between simulation and reality would indicate our input parameters are incorrect. We therefore consider our simulation, based on it's qualitative and quantitative similarity to the scanned track, to accurately represent the pattern of surface and sub-surface substrate deformation that occurred during the biplanar X-ray experiment.

Armed with this complete simulation of animated, deforming foot morphology and a deformable substrate responding to that foot, we are able to visualize and explore the formation of the track - its ontogeny - in a multitude of ways at and beneath the sediment surface (Fig. 7). Examining a sequence of time steps during the foot-substrate interaction allows us to visualize the temporal process of track development (Fig. 7A). Using randomized bands of colour oriented either vertically or horizontally, enables visualization of the directions and magnitudes of particle motion within the substrate (Figs. 7B and 7D). Color gradients can also be applied to individual particles, in order to visualize how far they move in various directions (Figs. 7C and 7E). Particle trajectories can be traced in order to track motions of individual particles or groups of particles within the substrate throughout the track forming process (Fig. 7F). For instance, selecting particles in the displacement rims and generating trajectories backwards, we can identify where the raised sediment has been pushed from. Subsurface layers can be exposed, presenting

transmitted undertracks (Fig. 7G). Ultimately there are countless directions that one can pursue to visualize track ontogeny, and understand how various aspects of track morphology were generated. We do not exhaustively list the possibilities here, but merely emphasize a variety of visualization techniques that can reveal previously hidden aspects of the track formation process.

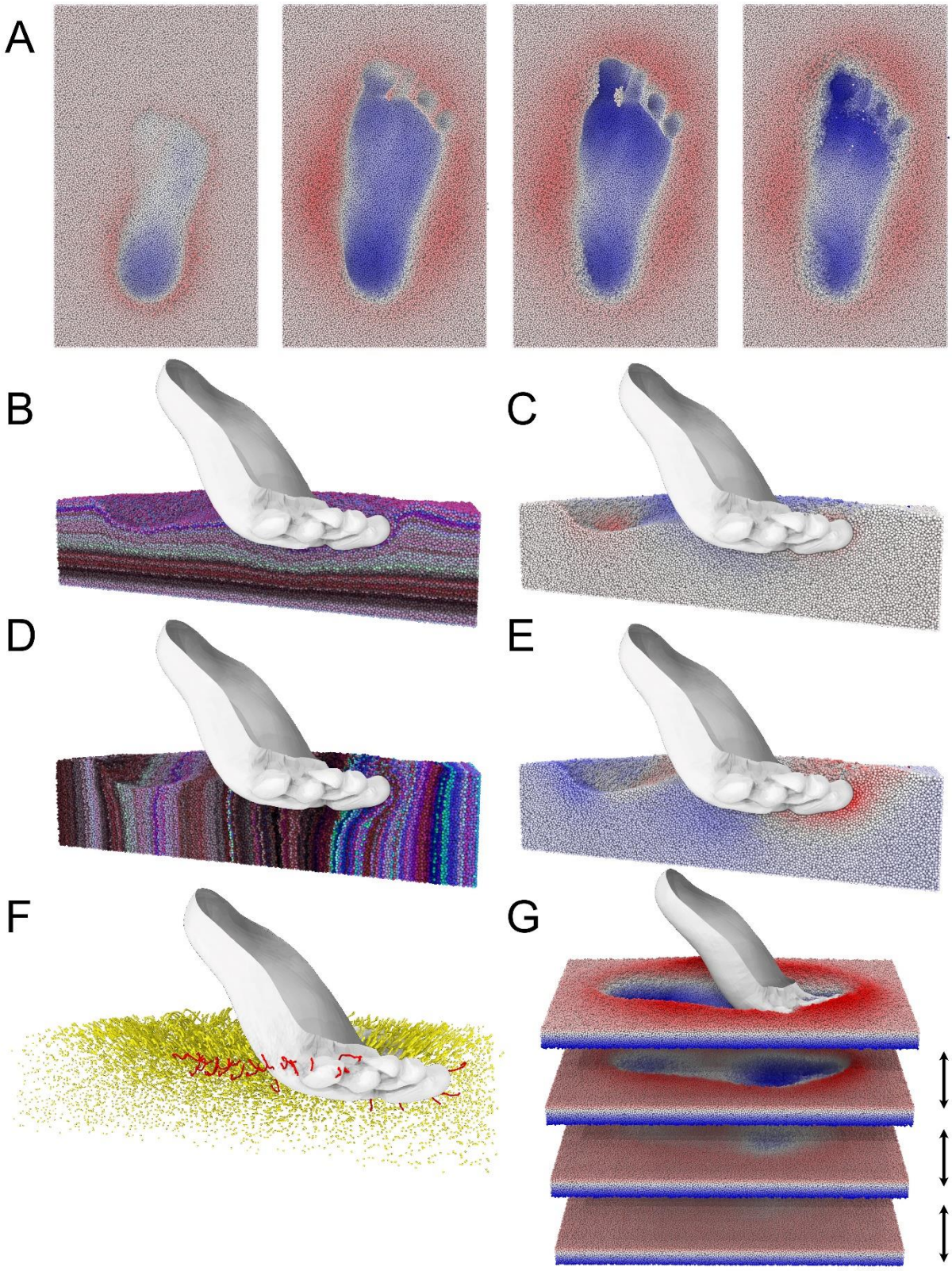

488

Figure 7. Examples of visualization methods applicable to our simulated tracks. A) Track ontogenetic sequence at ~25, 50, 75, and 100% of stance phase. Colour scale indicates height, and difference between darkest blue-red is 7 cm. B) Randomized horizontal colouring, exposed through longitudinal section, provides a view comparable with observing a laminated sediment. C) Medio-lateral motion of individual particles can be represented with colour, blue particles having moved medially, and red particles having moved laterally. D) and E) Visualize forward/backward motion of particles as either randomized vertical colouration (D) or colour-coded such that red indicates forward motion, blue indicates backward motion (E). F) Demonstrates particle vectors throughout the track forming process. Particles of interest, such as those in red which form the displacement rims, can be tracked separately and individually. G) The simulated track can be split at virtual bedding planes, exposing a sequence of penetrative and transmitted undertracks.

Conclusions

The combination of biplanar X-ray, 3-D animation, and particle simulation methods that we have introduced and applied here have the potential to inform a wide variety of research questions related to how locomotion varies across substrates with different mechanical properties, and how tracks can record those variations. Instruments that are ubiquitous to biomechanics labs, such as force plates, pressure pads, and optical motion capture systems, provide richly detailed understandings of how our feet function during locomotion. However, force- and pressure-sensing instruments are typically rigid and the opacity of feet and substrates conceal the interactions that occur at the foot-substrate interface, so these instruments are for the most part limited to studying locomotion on rigid surfaces. The hidden interactions between foot

512 and deformable substrate are of interest to researchers across many disciplines that seek to better
513 understand their mechanics. For example, in biorobotics, a great deal of attention has been
514 devoted to understanding how animals traverse irregular, deformable terrain. It has been
515 challenging to build robots that can navigate natural environments and their inherent
516 unpredictability, in part due to limited abilities to observe and measure mechanical interactions at
517 the foot-substrate interface (38,39). In human biomechanics, understandings of locomotion and
518 foot function across non-rigid substrates are similarly limited. It is known that humans alter their
519 kinematics on deformable substrates, and that the energetic costs of locomotion increase with
520 substrate compliance (40–42). However, it has been exceedingly difficult to observe and quantify
521 the manners in which human feet engage with non-rigid substrates. The methods described here
522 are transferable to these and other systems, and have the potential to open windows on
523 previously unobservable biomechanical phenomena. This emphasizes the interdisciplinarity that
524 is inherent to these approaches.

525 Within paleoanthropology, the methods developed here substantially expand the toolkit
526 that can be applied to analyze hominin tracks. Previous experimental studies, including our own,
527 have relied on the comparative method to determine whether and how various hominin tracks
528 differ from each other, and to develop anatomical and/or functional hypotheses for those
529 differences (9,11,43–48). The methods presented here focus instead on building knowledge of
530 human track ontogeny, in order to understand how particular anatomical or functional patterns
531 lead to the development of specific track morphologies. Through validated track simulation
532 methods, the combinations of foot anatomy and motion that would be capable of producing
533 particular fossil track morphologies can be reverse-engineered (28). When synthesized with
534 “functional” analyses of skeletal fossils (e.g., analyses of trabecular bone, cross-sectional

geometry, and/or articular morphology), these simulation-based analyses of fossil hominin tracks provide an unparalleled route to explicitly test and develop hypotheses regarding fossil hominin locomotion.

Acknowledgements

We thank David Baier, Beth Brainerd, Spencer Cheleden, Kay Fiske, Kia Huffman, Ben Knörlein, David Laidlaw, Kyra Tani Little, Armita Manafzadeh, Sabreen Megherhi, Johannes Novotny, David North, and Morgan Turner for assistance directly related to the design and implementation of this project. We also thank the anonymous volunteers who participated in these experiments.

Funding

This work was supported by the National Science Foundation (BCS-1825403 to KGH and PLF; BCS-1824821 to SMG) and Chatham University.

References

1. Darwin C. The descent of man, and selection in relation to sex. London: J. Murray; 1871. 898 p.
2. DeSilva J, McNutt E, Benoit J, Zipfel B. One small step: A review of Plio-Pleistocene hominin foot evolution. Am J Phys Anthropol. 2019;168:63–140.
3. Day MH, Napier JR. Fossil foot bones. Nature. 1964;201(4923):969–70.
4. Jungers WL, Harcourt-Smith WEH, Wunderlich RE, Tocheri MW, Larson SG, Sutikna T, et al. The foot of *Homo floresiensis*. Nature. 2009;459(7243):81–4.

5. Harcourt-Smith WEH, Throckmorton Z, Congdon KA, Zipfel B, Deane AS, Drapeau MSM, et al. The foot of *Homo naledi*. Nat Commun. 2015;6:1–8.
6. DeSilva JM, Gill CM, Prang TC, Bredella MA, Alemseged Z. A nearly complete foot from Dikika, Ethiopia and its implications for the ontogeny and function of *Australopithecus afarensis*. Sci Adv. 2018;4(7):eaar7723.
7. Gatesy SM, Middleton KM, Jenkins Jr. FA, Shubin NH. Three-dimensional preservation of foot movements in Triassic theropod dinosaurs. Nature. 1999;399:141–4.
8. Manafzadeh AR, Padian K. ROM mapping of ligamentous constraints on avian hip mobility: Implications for extinct ornithodirans. Proc R Soc B Biol Sci. 2018;285(1879).
9. Bennett MR, Harris JWK, Richmond BG, Braun DR, Mbua E, Kiura P, et al. Early hominin foot morphology based on 1.5-million-year-old footprints from Ileret, Kenya. Science. 2009;323(5918):1197–201.
10. Ashton N, Lewis SG, De Groote I, Duffy SM, Bates M, Bates R, et al. Hominin footprints from early Pleistocene deposits at Happisburgh, UK. PLoS One. 2014;9(2):e88329.
11. Hatala KG, Roach NT, Ostrofsky KR, Wunderlich RE, Dingwall HL, Villmoare BA, et al. Footprints reveal direct evidence of group behavior and locomotion in *Homo erectus*. Sci Rep. 2016;6:28766.
12. Hatala KG, Roach NT, Ostrofsky KR, Wunderlich RE, Dingwall HL, Villmoare BA, et al. Hominin track assemblages from Okote Member deposits near Ileret,

Kenya, and their implications for understanding fossil hominin paleobiology at 1.5 Ma. J Hum Evol. 2017;112:93–104.

13. Masao FT, Ichumbaki EB, Cherin M, Barili A, Boschian G, Iurino DA, et al. New footprints from Laetoli (Tanzania) provide evidence for marked body size variation in early hominins. eLife. 2016;5:29.

14. Altamura F, Bennett MR, D'Août K, Gaudzinski-Windheuser S, Melis RT, Reynolds SC, et al. Archaeology and ichnology at Gombore II-2, Melka Kunture, Ethiopia: everyday life of a mixed-age hominin group 700,000 years ago. Sci Rep. 2018;8(1):1–11.

15. Altamura F, Bennett MR, Marchetti L, Melis RT, Reynolds SC, Mussi M. Ichnological and archaeological evidence from Gombore II OAM, Melka Kunture, Ethiopia: An integrated approach to reconstruct local environments and biological presences between 1.2 and 0.85 Ma. Quat Sci Rev. 2020;244:106506.

16. Bennett MR, Falkingham P, Morse SA, Bates K, Crompton RH. Preserving the impossible: Conservation of soft-sediment hominin footprint sites and strategies for three-dimensional digital data capture. PLoS One. 2013;8(4).

17. Falkingham PL, Bates KT, Avanzini M, Bennett MR, Bordy EM, Breithaupt BH, et al. A standard protocol for documenting modern and fossil ichnological data. Palaeontology. 2018;

18. Minter NJ, Braddy SJ, Davis RB. Between a rock and a hard place: Arthropod trackways and ichnotaxonomy. Lethaia. 2007;40(4):365–75.

19. Padian K, Olsen PE. The fossil trackway *Pteraichnus*: not pterosaurian, but crocodilian. J Paleontol. 1984;178–84.

20. Falkingham PL. Interpreting ecology and behaviour from the vertebrate fossil track record. J Zool. 2014;292(4):222–8.
21. Morse SA, Bennett MR, Liutkus-Pierce C, Thackeray JF, McClymont J, Savage R, et al. Holocene footprints in Namibia: the influence of substrate on footprint variability. Am J Phys Anthropol. 2013;151(2):265–79.
22. Falkingham PL, Gatesy SM. The birth of a dinosaur footprint: Subsurface 3D motion reconstruction and discrete element simulation reveal track ontogeny. Proc Natl Acad Sci. 2014;111(51):18279–84.
23. Maladen R, Ding Y, Li C, Goldman DI. Undulatory swimming in sand: Subsurface locomotion of the sandfish lizard. Science. 2009;325(5938):314–8.
24. Ellis RG, Gatesy SM. A biplanar X-ray method for three-dimensional analysis of track formation. Palaeontol Electron. 2013;16(1):1T.
25. Hatala KG, Perry DA, Gatesy SM. A biplanar X-ray approach for studying the 3D dynamics of human track formation. J Hum Evol. 2018;121:104-18.
26. Cundall PA, Strack ODL. A discrete numerical model for granular assemblies. Géotechnique. 1979;29:47–65.
27. Kloss C, Goniva C. LIGGGHTS - Open source discrete element simulations of granular materials based on Lammps. In: TMS, editor. Supplemental Proceedings: Materials Fabrication, Properties, Characterization, and Modeling, Volume 2. Hoboken: John Wiley & Sons, Inc; 2011. p. 781–8.
28. Falkingham PL, Turner ML, Gatesy SM. Constructing and testing hypotheses of dinosaur foot motions from fossil tracks using digitization and simulation. Palaeontology. 2020;1–16.

29. Gatesy SM, Falkingham PL. Neither bones nor feet: track morphological variation and 'preservation quality.' J Vertebr Paleontol. 2017;e1314298.
30. Brainerd EL, Baier DB, Gatesy SM, Hedrick TL, Metzger KA, Gilbert SL, et al. X-ray reconstruction of moving morphology (XROMM): precision, accuracy and applications in comparative biomechanics research. J Exp Zool A. 2010;313(5):262–79.
31. Knörlein BJ, Baier DB, Gatesy SM, Laurence-Chasen JD, Brainerd EL. Validation of XMALab software for marker-based XROMM. J Exp Biol. 2016;219(23):3701–11.
32. Baier DB. XROMM Maya Tools. 2018. Available from: https://bitbucket.org/xromm/xromm_mayatools/src/master/
33. Stukowski A. Visualization and analysis of atomistic simulation data with OVITO - the Open Visualization Tool. Modelling Simul Mater Sci Eng. 2010;18:015012.
34. De Clercq D, Aerts P, Kunnen M. The mechanical characteristics of the human heel pad during foot strike in running: An in vivo cineradiographic study. J Biomech. 1994;27(10):1213–22.
35. Gefen A, Megido-Ravid M, Itzchak Y. In vivo biomechanical behavior of the human heel pad during the stance phase of gait. J Biomech. 2001;34:1661–1665.
36. Chi KJ, Schmitt D. Mechanical energy and effective foot mass during impact loading of walking and running. J Biomech. 2005;38(7):1387–95.
37. Caravaggi P, Pataky T, Gunther M, Savage R, Crompton R. Dynamics of longitudinal arch support in relation to walking speed: contribution of the plantar aponeurosis. J Anat. 2010;217(3):254–61.

38. Ijspeert AJ. Biorobotics: using robots to emulate and investigate agile locomotion. Science. 2014;346(6206):196–203.
39. Aguilar J, Zhang T, Qian F, Kingsbury M, McInroe B, Mazouchova N, et al. A review on locomotion robophysics: The study of movement at the intersection of robotics, soft matter and dynamical systems. Reports Prog Phys. 2016;79(11):110001.
40. Ferris DP, Louie M, Farley CT. Running in the real world: Adjusting leg stiffness for different surfaces. Proc R Soc B Biol Sci. 1998;265(1400):989–94.
41. Lejeune TM, Willems PA, Heglund NC. Mechanics and energetics of human locomotion on sand. J Exp Biol. 1998;201:2071–80.
42. Kerdok AE, Biewener AA, McMahon TA, Weyand PG, Herr HM. Energetics and mechanics of human running on surfaces of different stiffnesses. J Appl Physiol. 2002;92(2):469–78.
43. Day MH, Wickens EH. Laetoli Pliocene hominid footprints and bipedalism. Nature. 1980;286:385–7.
44. Tuttle RH, Webb DM, Weidl E, Baksh M. Further progress on the Laetoli trails. J Archaeol Sci. 1990;17:347–62.
45. Meldrum DJ. Midfoot Flexibility, Fossil Footprints, and Sasquatch Steps: New Perspectives on the Evolution of Bipedalism. J Sci Explor. 2004;18(1):65–79.
46. Raichlen DA, Gordon AD, Harcourt-Smith WEH, Foster AD, Haas WR. Laetoli footprints preserve earliest direct evidence of human-like bipedal biomechanics. PLoS One. 2010;5(3):e9769.

671 47. Crompton RH, Pataky TC, Savage R, D'Août K, Bennett MR, Day MH, et al.
672 Human-like external function of the foot, and fully upright gait, confirmed in the
673 3.66 million year old Laetoli hominin footprints by topographic statistics,
674 experimental footprint-formation and computer simulation. J R Soc Interface.
675 2012;9(69):707–19.
676 48. Hatala KG, Demes B, Richmond BG. Laetoli footprints reveal bipedal gait
677 biomechanics different from those of modern humans and chimpanzees. Proc R Soc
678 B. 2016;283:20160235.